

Do MLLMs Really See It: Reinforcing Visual Attention in Multimodal LLMs

Siqu Ou^{1,2*} Tianrui Wan^{1,3} Zhiyuan Zhao¹ Junyu Gao^{1,3} Xuelong Li¹

Abstract

While chain-of-thought (CoT) reasoning has substantially improved multimodal large language models (MLLMs) on complex reasoning tasks, existing approaches largely rely on long textual reasoning trajectories and provide limited mechanisms for learning stable visual attention policies. Our analysis shows that current MLLMs exhibit weak visual focus: early-stage visual misalignment is rarely corrected during subsequent reasoning, leading to error propagation and failed inferences. We argue that this limitation stems from inadequate credit assignment for visual attention during training. To address this issue, we propose SAYO, a visual reasoning model trained with a reinforcement learning (RL) framework that introduces a region-level visual attention-based reward. This reward explicitly aligns optimization signals with visually grounded reasoning steps, enabling the model to learn more reliable attention behaviors. Extensive experiments across multiple multimodal benchmarks demonstrate that SAYO consistently improves performance on diverse reasoning and perception tasks.

1. Introduction

Recent advances in multimodal large language models (MLLMs) (Bai et al., 2025; Wang et al., 2025c; Huang et al., 2026) have significantly improved performance on complex reasoning tasks that require integrating visual and linguistic information. In particular, chain-of-thought (CoT) reasoning has emerged as an effective mechanism for decomposing complex problems into sequential inference steps (Yang et al., 2023; Xu et al., 2025). Despite these successes, existing MLLMs continue to exhibit fundamental limitations when reasoning over visually complex inputs, especially in scenarios requiring precise and sustained visual grounding

*Work done during an internship at TeleAI ¹TeleAI
²Shanghai Jiao Tong University ³Northwestern Polytechnical University. Correspondence to: Zhiyuan Zhao <zhaozhiyuan27@chinatelecom.cn>, Xuelong Li <xuelong_li@ieee.org>.

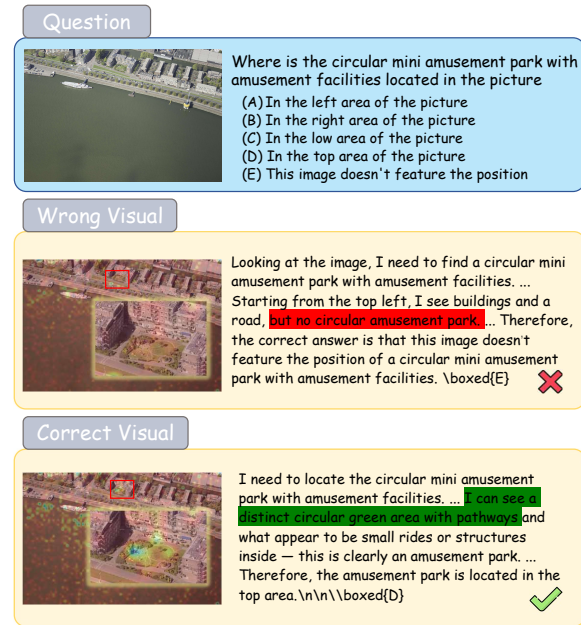


Figure 1. In the reasoning process of CoT, initial visual focusing errors can mislead the inference processing. We emphasize enhancing the model’s visual capabilities to ensure MLLMs can proactively focus on text-relevant visual regions. The resolution of image is 2752x1824. The attention map displays the average attention of all generated tokens.

across long reasoning trajectories. Most prior approaches emphasize textual reasoning processes or rely on heuristic visual prompt engineering, such as programmatic region highlighting or prompt reflection mechanisms (Yang et al., 2025b). While these methods can indirectly influence visual perception, they do not explicitly address how visual attention behaviors are learned during training. Prior works have begun to probe this problem that current MLLMs often develop unstable visual attention policies, particularly when confronted with complex multi-object scenes or information-dense documents (Liu et al., 2025b; Yang et al., 2025a). These findings suggest that MLLMs may struggle to focus their visual attention and become distracted by an excess of other visual signals. Although techniques such as ViP (Cai et al., 2024) introduce visual cues to mark regions of interest, their effectiveness ultimately depends on the model’s pre-existing attention behavior, which remains insufficiently

optimized.

Previous studies (Tong et al., 2024; Verma et al., 2024) have revealed a consistent pattern: when an MLLM attends to incorrect visual regions at early inference stages, this misalignment is rarely corrected during subsequent reasoning. Instead, erroneous visual assumptions propagate through the chain of thought, leading to systematic inference failures. This phenomenon is especially pronounced in long reasoning sequences, where early errors exert a disproportionate influence on final predictions. We argue that this limitation reflects a broader optimization deficiency, rather than a lack of representational capacity. Specifically, existing training objectives fail to provide effective credit assignment signals for learning reliable visual attention behaviors during multimodal reasoning.

To investigate this issue, we evaluate representative MLLMs on challenging visual question answering benchmarks involving complex multi-object scenes. As shown in Figure 1, analysis indicates that incorrect predictions are frequently accompanied by misplaced attention or inaccurate spatial localization. Quantitatively, we observe a strong correlation between visual attention accuracy and overall task performance, supporting the hypothesis that attention misalignment is a primary driver of reasoning errors.

Motivated by these findings, we propose Entropy-Based Target Attention Reward, a novel reinforcement learning-based framework designed to improve visual attention learning in MLLMs. Rather than relying on external visual prompts or architectural modifications, it introduces an attention-aware reward that directly aligns optimization signals with visually grounded reasoning steps. The reward is selectively applied based on token-level entropy, encouraging the model to prioritize visual information at decision points where uncertainty is highest. From a learning perspective, this design provides a principled mechanism for addressing credit assignment in multimodal reasoning. As illustrated in Figure 1, models trained with this reward exhibit significantly improved attention alignment during inference, consistently focusing on task-relevant visual regions at critical reasoning steps. Importantly, this improvement emerges without requiring explicit visual prompts, special tokens, or iterative prompt refinement at inference time. The resulting model is able to maintain stable visual grounding throughout long reasoning trajectories.

In summary, this paper makes the following contributions:

- **An optimization-centric analysis of visual attention in MLLMs.** We identify visual attention misalignment as a credit assignment failure and demonstrate that long chains of thought struggle to recover from early attention errors.
- **A reinforcement learning framework for visual at-**

tention learning. We propose Entropy-Based Target Attention Reward, which introduces an entropy-selective, attention-based reward to enable stable and sustained visual grounding during multimodal reasoning.

- **A strong and generalizable visual reasoning model.** Using the proposed framework, we train SAYO and show consistent improvements across diverse multimodal benchmarks, demonstrating strong generalization in both reasoning and perception tasks.

2. Related Works

2.1. MultiModal Large Language Models

Multimodal Large Language Models (Huang et al., 2026; Team et al., 2025) have made remarkable progress by integrating various modalities—such as text, images, and video—into a unified framework for understanding and reasoning. In this framework, different modality encoders project inputs into a shared semantic space, which is then processed by a language model to generate responses. However, although most existing MLLMs possess powerful reasoning capabilities, they struggle to pinpoint the truly relevant parts within complex visual information accurately (Liu et al., 2025b). This prevents the reasoning capabilities of MLLMs from being effectively utilized.

2.2. Enhance Visual Reasoning

A significant recent trend in research involves explicitly applying visual processing to images using external tools (e.g., Python programs) before inputting them into models, such as resizing images or adding bounding boxes around target objects. Studies indicate that such methods can significantly impact the performance of MLLMs, particularly in tasks like visual localization. Recent studies, such as Visual SketchPad (Hu et al., 2024), ReFocus (Fu et al., 2025), and ControlMLLM (Wu et al., 2025) have explored the performance of visual cueing frameworks across various visual comprehension tasks. However, these methods rely on where MLLMs locate visual prompts for processing. BLINK (Fu et al., 2024) indicates that most open-source multimodal language models struggle to comprehend visual prompts, and incorrect localization undermines their effectiveness. Furthermore, constrained by the fixed nature of the procedures, the aforementioned methods face challenges in transferring to new visual reasoning tasks.

2.3. Strengthen Visual Focus

Consistent with our proposed visual focus, recent research (Yang et al., 2025a; Zhang et al., 2025a) emphasizes the importance of enhancing attention to visual cues

in long-chain reasoning. (Chen et al., 2025) discovered that the model’s overreliance on prior language led to neglect of visual details in dense information tasks. Look-Back (Yang et al., 2025b) enhances the focus of the thinking process on images by incorporating look-back labels into long-term reasoning chains. Building upon this foundation, Reflection-V (Jian et al., 2025) further introduces an attention reward mechanism. By rewarding the overall attention of the thought chain text toward the image, it promotes the discovery of visual information. Unlike the aforementioned methods, we leverage data annotated with visual bounding boxes to enhance the visual attention capabilities of RL-trained MLLMs. The resulting MLLMs maintain visual focus and reasoning on target objects without requiring lengthy textual inference and reflection processes.

3. Do MLLMs Know where to focus?

Recent studies suggest that multimodal large language models (MLLMs) frequently fail to attend to the correct visual regions during long-chain reasoning, resulting in systematic inference errors. This observation raises two key questions: (i) whether current MLLMs are able to accurately localize target objects in complex multi-object scenes, and (ii) how visual attention misalignment affects downstream reasoning performance. To answer these questions, we conduct a diagnostic analysis on the GQA (Hudson & Manning, 2019) dataset, focusing on the relationship between visual attention and model accuracy.

As shown in Figure 1, attention alignment plays a critical role in inference quality: directing attention to the correct visual regions significantly improves prediction accuracy. To quantitatively characterize this effect, we introduce a target attention ratio, which measures the extent to which a model allocates visual attention to the target object relative to irrelevant image regions.

We extract attention weights from the final transformer layer, where multimodal fusion is fully realized. Let $\alpha_{t_i, t_g}^{(h)}$ denote the attention weight from generated token t_g to image token p at attention head h . We denote by $\mathcal{T}_{\text{target}}$ the set of image tokens corresponding to the target region and by \mathcal{T}_{all} those corresponding to entire image regions. For each generated token t_g , we compute the average attention mass assigned to the target and entire image regions, then we average across all attention heads to obtain the overall target attention score a and entire image attention score v , respectively:

$$a = \frac{1}{H} \sum_{h=1}^H \frac{1}{|\mathcal{T}_{\text{target}}|} \sum_{t_i \in \mathcal{T}_{\text{target}}} \alpha_{t_i, t_g}^{(h)}, \quad (1)$$

$$v = \frac{1}{H} \sum_{h=1}^H \frac{1}{|\mathcal{T}_{\text{all}}|} \sum_{t_i \in \mathcal{T}_{\text{all}}} \alpha_{t_i, t_g}^{(h)}. \quad (2)$$

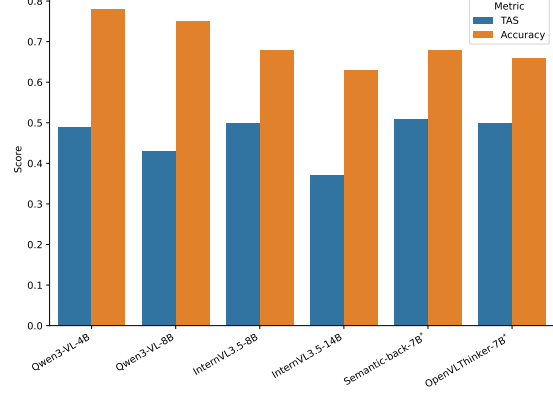


Figure 2. Comparison of target attention score (TAS) and accuracy across Models on a part of GQA dataset. The displayed score and accuracy represent the average across all samples. * denotes models based on the Qwen2.5-7B series.

Based on these quantities, we define a normalized attention advantage score to quantify visual focus:

$$R_a = \frac{1}{2} \left(1 + \tanh \left(\log \frac{a + \varepsilon}{v + \varepsilon} \right) \right) \quad (3)$$

where ε is a small constant used for numerical stability.

As shown in Figure 2, experiments across multiple visual models reveal a strong positive correlation between target attention scores and response accuracy. For models within the same series, higher attention weights on the target visual region yield better inference performance. Notably, despite recent advances in reinforcement learning-based optimization for MLLMs, all evaluated models exhibit consistently low target attention scores. This suggests that while existing RL techniques improve textual reasoning trajectories, they fail to provide effective learning signals for precise visual focus. Consequently, models may develop strong abstract reasoning capabilities without reliably grounding their inferences in the correct visual evidence, fundamentally limiting their visual reasoning performance.

4. Method

In the analysis behind, we observe that current models exhibit insufficient attention to target visual information. This deficiency in visual information utilization severely limits their powerful reasoning capabilities when addressing visual reasoning problems. To address this issue, we propose a reinforcement learning reward training strategy based on visual attention. First, we constructed training data emphasizing visual attention focus using visual reasoning datasets with detailed object annotation information. Subsequently, we employed GRPO to incentivize attention toward target visual signals through reward function.

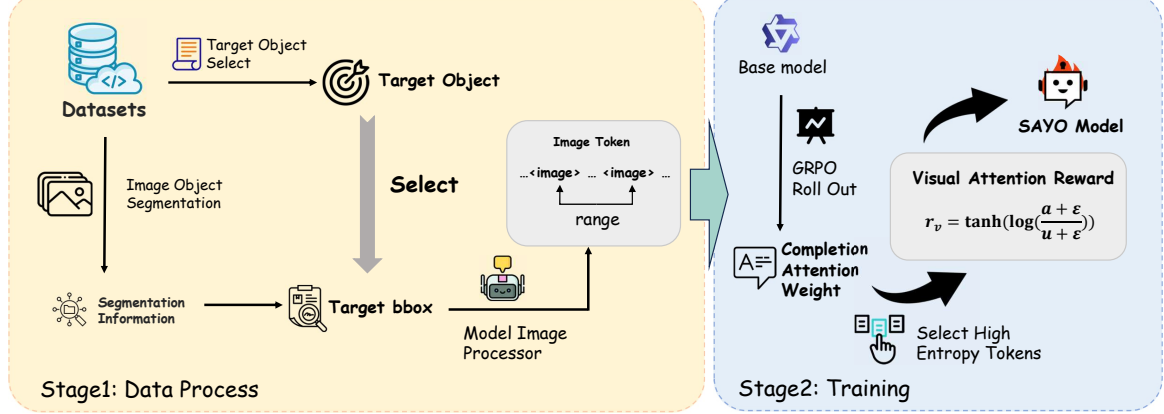


Figure 3. The workflow for our method, including constructing reasoning data with region visual information and training with region attention reward

4.1. Construction of Data with Visual Focus

Existing large visual language model training paradigms typically focus solely on the accuracy and formatting compliance of model responses and evaluation accordingly. The neglect of visual attention shifts during reasoning processes prevents these data from demonstrating the visual attention focus we propose. Inspired by recent visual prompt studies, we employ a precisely designed toolchain that aligns textual questions with visual token information to accomplish data construction tasks. The data construction process is detailed in the following.

As shown in Figure 3, in the first stage, we extract the final target object text from the question-answer pairs and match it with image segmentation information to obtain bounding box coordinates. Subsequently, based on the model’s image processing methodology, we convert the bounding boxes into corresponding visual token ranges. This process yields the objects eligible for visual attention rewards.

4.2. Visual Attention Based Reward

Following previous studies, we employ the reinforcement learning algorithm GRPO to enhance the perception, localization, and reasoning capabilities of visual models. Building upon the original format reward, we have introduced a new reward mechanism based on target visual attention. This aims to incentivize the model to accurately focus on the correct visual tokens. Based on the analyses in Section 3, model’s attention to target visual regions is positively correlated with accuracy.

Furthermore, prior research (Wang et al., 2025b;a) shows that a small number of high-entropy tokens contain more information. If only these information-rich tokens are selected as training targets, better performance results can be achieved. Why does optimizing attention on high-

entropy tokens lead to generalized reasoning improvements? We formalize the reasoning process as a trajectory $\tau = (v, q, t_1, t_2, \dots, t_T)$. For a high-entropy token $t_k \in \mathcal{Q}_{high}$, the model exhibits high epistemic uncertainty, often stemming from insufficient grounding in the visual context v . Standard Next-Token Prediction (NTP) minimizes $-\log p(t_k|v, t_{<k})$, allowing the model to bypass visual verification by relying on linguistic priors (hallucination). In contrast, our SAYO objective explicitly penalizes this behavior. By enforcing high Attention Ratio R_a specifically at high-entropy states, we impose a visual verification constraint:

$$\mathcal{L}_{SAYO} = \mathbb{E}_{t \sim \pi}[r_v(a_t) \cdot \nabla \log \pi(t|s)] \quad (4)$$

where r_v acts as a regularizer that forces the policy to resolve uncertainty by consulting the visual evidence. This mechanism effectively suppresses “blind” reasoning. We argue that this “Look-to-Verify” policy is a domain-agnostic metaskill. Once the model learns to ground its attention in complex natural scenes (dense objects) and charts (structured elements), this attention-sharpening capability naturally transfers to other visual domains, such as geometric diagrams, ensuring that the pre-trained mathematical reasoning engine operates on correctly perceived visual primitives.

Based on these findings, we designed the following reward rules: Let \mathcal{Q}_{high} denote the set of generated tokens whose entropies rank in the top 30% among all generated tokens. Using attention weights from the final transformer layer (Jian et al., 2025), we compute the average attention mass from the selected tokens to the target visual region and to all visual tokens, respectively:

$$a_g = \frac{1}{|\mathcal{Q}_{high}|} \sum_{t_g \in \mathcal{Q}_{high}} \frac{1}{H} \sum_{h=1}^H \frac{1}{|\mathcal{T}_{target}|} \sum_{t_i \in \mathcal{T}_{target}} \alpha_{t_i, t_g}^{(h)}, \quad (5)$$

Table 1. Performance of SAYO across various visual reasoning benchmarks with different tasks. \dagger indicates results are taken from the respective models’ official reports. The best results of each benchmark among open-source models are **bold** and the secondary results are underlined.

Model	General				Math			Chart		Avg
	MMERealWorld	M3CoT	V*	MMStar	MathVision	We-Math	ChartQA	AI2D	CharXiv	
<i>Close-Source Models</i>										
GPT4o	73.06	74.20 \dagger	-	64.70 \dagger	30.40 \dagger	69.00 \dagger	75.32	84.60	48.90 \dagger	-
Gemini 2.5 Pro	-	-	83.80 \dagger	77.50 \dagger	-	80.60 \dagger	83.30 \dagger	90.90 \dagger	-	-
<i>Open-Source General Models</i>										
Qwen3-VL-4B	56.80	65.10	79.06	60.80	21.64	55.63	80.12	75.16	38.00	59.15
Qwen3-VL-8B	56.23	64.71	81.15	62.60	22.20	52.64	78.96	75.55	42.70	59.64
Qwen3-VL-30B-A3B	43.72	56.86	52.88	53.73	22.93	54.66	78.42	71.76	39.80	52.75
InternVL3.5-8B	45.34	54.70	73.82	60.27	13.82	20.06	79.12	73.22	34.10	50.49
InternVL3.5-14B	48.57	51.86	70.16	55.93	13.85	33.10	81.76	69.43	38.90	51.51
InternVL3.5-30B-A3B	38.61	55.65	72.25	58.33	17.07	44.89	81.20	78.47	33.70	52.73
InternVL3.5-38B	54.56	53.75	79.58	54.20	13.36	24.20	81.60	75.10	44.40	53.42
Kimi-VL-16B	42.00	54.01	75.39	63.47	17.50	42.01	82.08	77.04	31.30	53.87
<i>Open-Source Reasoning Models</i>										
ViGoRL	55.34	68.72	60.73	61.53	22.07	62.01	59.64	79.70	30.40	55.57
OpenVLThinker-7B	48.31	63.29	80.10	63.07	25.59	64.48	75.44	<u>82.61</u>	35.20	59.79
Semantic-back-7B	46.43	67.77	78.01	63.07	<u>27.57</u>	<u>66.61</u>	82.32	81.74	38.10	61.29
R1-Onenision-7B	44.87	61.73	57.07	57.00	29.90\dagger	61.80 \dagger	42.72	74.45	20.90	50.50
NoisyRollout-7B	51.69	67.90	76.96	<u>63.67</u>	22.01	70.57	82.16	80.73	40.50	61.80
<i>Ours Trained Model</i>										
SAYO-Qwen-4B	<u>57.63</u>	64.32	83.25	63.53	22.47	63.97	81.96	80.51	41.90	62.17
SAYO-Qwen-8B	62.85	<u>68.46</u>	<u>82.20</u>	65.27	25.26	64.83	81.84	83.06	42.50	64.03
SAYO-InternVL-8B	50.03	57.20	72.77	62.73	13.62	25.23	<u>82.28</u>	76.88	<u>43.20</u>	53.77

$$v_q = \frac{1}{|\mathcal{Q}_{\text{high}}|} \sum_{t_g \in \mathcal{Q}_{\text{high}}} \frac{1}{H} \sum_{h=1}^H \frac{1}{|\mathcal{T}_{\text{all}}|} \sum_{t_i \in \mathcal{T}_{\text{all}}} \alpha_{t_i, t_g}^{(h)}. \quad (6)$$

Therefore, the visual attention-based reward is given by:

$$r_v = \tanh \left(\log \frac{a_q + \varepsilon}{v_q + \varepsilon} \right), \quad (7)$$

where ε is a small constant for numerical stability. The reward $r \in (-1, 1)$ reflects whether the model allocates relatively more attention to the target region than to the visual context as a whole. The overall reward r_o in GRPO is the weighted sum of the region visual attention-based reward r_v and format reward r_f (Shao et al., 2024), the equation is given as: $r_o = r_v + r_f$

5. Experiments

5.1. Experimental Setup

Implementations. To evaluate our method, we use Qwen3-VL (Bai et al., 2025) and InternVL3.5-8B (Wang

et al., 2025c) as the base model. During the training stage, we trained the model using GRPO with entropy and visual attention-based reward for 4 epochs on 6 NVIDIA H200 GPUs, based on the TRL (von Werra et al., 2020) framework. The detailed composition of training data is shown in Appendix C. Training details are provided in Appendix A.

Benchmarks. We conducted detailed analytical experiments to evaluate how our approach enhances the model’s visual reasoning capabilities. To ensure thoroughness in our assessment, we selected multiple widely recognized visual understanding benchmarks across various domains. These benchmarks encompass structured image reasoning, mathematical reasoning, and general visual reasoning. For evaluating mathematical reasoning, we adopt We-Math (Qiao et al., 2025) and MathVision (Wang et al., 2024a). To evaluate performance across general visual reasoning, we utilize M3CoT (Chen et al., 2024b), V*Bench (Wu & Xie, 2024), MMStar (Chen et al., 2024a), and MME-RealWorld-Lite (Zhang et al., 2025b). Notably, MME-RealWorld also focuses on assessing the model’s performance in

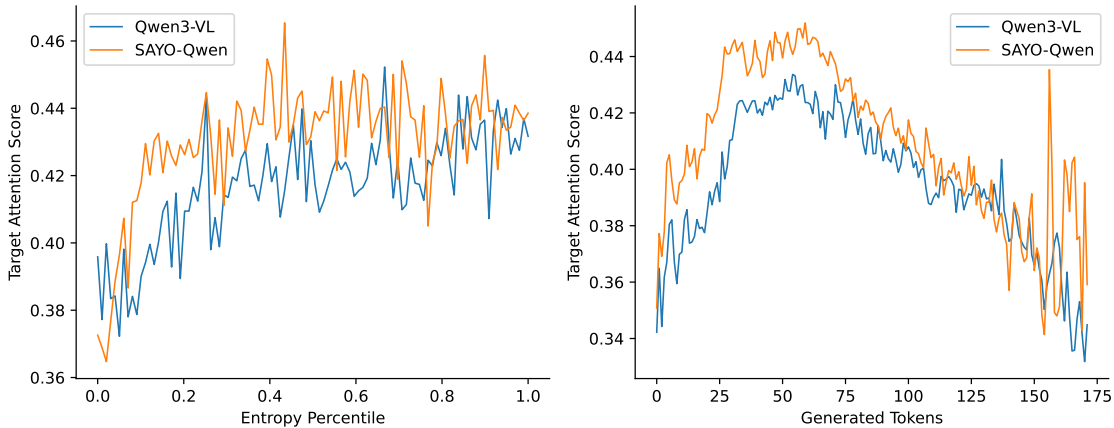


Figure 4. Attention weights of model-generated tokens to target visual tokens (last layer) and attention weights of tokens with different entropy values to target visual tokens. The entropy values shown have been normalized across samples, and the displayed attention weights represent the average across all samples.

complex, high-resolution image reasoning. Furthermore, ChartQA (Masry et al., 2022), CharXiv (Wang et al., 2024b), and AI2D (Kembhavi et al., 2016) are used to assess structured image reasoning ability, as they cover a broad range of chart understanding questions. Additionally, we compared SAYO against various of baselines: (i) close-source MLLMs such as GPT-4o (OpenAI) and Gemini 2.5 pro (Comanici et al., 2025); (ii) open-source general MLLMs, such as Qwen3-VL (Bai et al., 2025), InternVL3.5 (Wang et al., 2025c), and Kimi-VL-16B (Team et al., 2025); (iii) open-source reasoning MLLMs, such as OpenVLThinker-7B (Deng et al., 2025), Semantic-back-7B (Yang et al., 2025b), ViGoRL (Sarch et al., 2025), NoisyRollout-Geo3k-7B (Liu et al., 2025a), and R1-Onevision-7B (Yang et al., 2025c).

5.2. Main Results

We evaluate the performance of our model, SAYO, on various of visual reasoning benchmarks across three categories: visual math problems, structured image problems, and general reasoning. As shown in Table 1, the results indicate that our model significantly outperforms base models and other open-source models of a similar scale in terms of reasoning capability. Compared to models trained using other methods, SAYO also demonstrates significant performance advantages. Notably, SAYO outperformed some closed-source models and larger open-source models on certain benchmarks. For example, on MMStar, SAYO-Qwen outperforms Kimi-VL-16B and GPT-4o. In contrast to existing reasoning MLLMs, which show improved math reasoning but a decline in general reasoning capabilities, SAYO yields significant improvements across a variety of reasoning tasks. Besides, experimental results show that our proposed method is effective across different models and

various scales.

A counter-intuitive finding in Table 1 is the significant improvement on We-Math and MathVision, despite the exclusion of mathematical datasets from our training phase. We attribute this cross-domain generalization to the decoupling of visual parsing and logical reasoning. Current state-of-the-art base models (e.g., Qwen-VL) already possess strong latent mathematical reasoning capabilities derived from massive textual pre-training. However, their performance is often bottlenecked by visual misalignment, e.g., attending to the wrong geometric line or misreading a chart axis—which propagates errors into the reasoning chain. By training on ReFocus datasets (structured documents) and GQA (dense scenes), SAYO learns a robust structure-aware attention policy. By correcting the input signal (i.e., ensuring the model “sees” the correct triangle side), SAYO effectively eliminates the garbage in phase. This allows the model’s pre-existing mathematical engine to process valid visual premises, thereby unlocking performance gains without explicit domain-specific training. Thus, the improvement is not due to learning new mathematics, but due to the precise grounding of visual premises required for mathematical deduction.

5.3. Ablation Study

Effectiveness of attention reward. To systematically assess the contribution of the proposed regional visual attention-based reward, we conduct a series of controlled ablation experiments designed to isolate its effect from other reward components. Specifically, we consider the following variants: (i) Accuracy-only reward, where the attention-based reward is replaced by a conventional answer accuracy reward; (ii) Attention-only reward, where optimization relies solely on the proposed visual attention reward; (iii)

Table 2. Ablation results for different combinations of rewards and visual attention-based reward on performance improvement. Attn. Reward denotes visual attention-based reward, and Acc. Reward denotes accuracy reward. All combinations include format rewards.

Model	General				Math				Chart		Avg
	MMERealWorld	M3CoT	Vstar	MMStar	MathVision	We-Math	ChartQA	AI2D	CharXiv		
Qwen3-VL-8B	56.23	64.71	81.15	62.60	22.20	52.64	78.96	75.55	42.70	59.64	
	62.85	67.86	82.20	65.27	25.26	64.83	81.84	83.06	42.50	63.96	
	57.01	65.96	78.01	65.20	23.59	56.61	82.52	78.01	41.40	60.92	
	61.59	67.77	82.20	66.00	25.95	66.15	82.56	83.03	43.20	64.27	
InternVL3.5-8B	45.34	54.70	73.82	60.27	13.82	20.06	79.12	73.22	34.10	50.49	
	50.03	57.20	72.77	62.73	13.62	25.23	82.28	76.88	43.20	53.77	
	47.94	57.16	74.35	62.20	14.05	24.31	82.68	75.62	41.60	53.32	
	49.04	56.77	74.35	63.73	14.14	27.24	82.04	76.81	42.80	54.10	

Combined reward, where both attention-based and accuracy rewards are applied.

The results, summarized in Table 2, demonstrate that incorporating a visual attention-based reward leads to substantial and consistent performance improvements across all evaluated benchmarks. Notably, models trained using only the visual attention reward achieve performance comparable to those trained with the combined reward, whereas models trained with accuracy rewards alone exhibit only marginal gains. This indicates that models with weaker knowledge still face performance gaps due to limitations in their reasoning capabilities.

These findings suggest that deficiencies in current MLLMs stem less from limited reasoning capacity and more from insufficient visual perception and localization. In other words, while existing models are capable of performing complex reasoning once relevant information is identified, they frequently fail to reliably extract and attend to the necessary visual evidence. By explicitly incentivizing correct visual focus, the proposed attention reward effectively unlocks the model’s latent reasoning capabilities, leading to more accurate and robust inference.

How to Design an Effective Attention Reward Beyond validating the necessity of the attention-based reward, we further investigate how different design choices affect its effectiveness. We evaluate several reward configurations that vary in token selection strategy and reward granularity, as reported in Table 3. Across all settings, introducing visual attention-based supervision consistently improves performance, confirming the general effectiveness of this approach.

A key observation is that selectively rewarding a subset of high-information tokens yields significantly larger performance gains than applying rewards uniformly across all tokens. This result aligns with the intuition that not all tokens contribute equally to visual grounding during multimodal reasoning. Many tokens serve primarily syntactic or

connective roles and do not require direct visual attention. Including such low-information tokens in reward computation introduces noise, weakening the learning signal and potentially destabilizing policy optimization.

Further analysis of the training dynamics reveals that entropy-selective token rewards lead to more stable and faster convergence, as evidenced by reduced variance in training rewards and improved consistency across runs. By focusing the reward on tokens that correspond to critical decision points—where visual evidence is most relevant—the model receives clearer and more informative supervision. Additional analyses of training stability and convergence behavior are provided in Appendix D and E.

5.4. Results Analysis

In Section 3, we demonstrate that existing MLLMs exhibit shortcomings in terms of accurate visual perception capabilities through attention advantage score R_a . Based on this metric, we will analyze in this section whether the performance improvement of SAYO truly stems from the training strategy targeting regional visual attention, and what changes this training strategy brings to the model.

We compared the target visual attention score R_a between Qwen3-VL-8B-Instruct and SAYO-Qwen-8B on the same task. As shown in Figure 4, we found that throughout the generated token sequence, SAYO consistently exhibited significantly higher visual attention weights toward the target region than Qwen3-VL, and significantly enhanced attention to the target region of the image during the later stages of inference when generating answers. Additionally, to verify whether this method can effectively improve the attention of high-entropy tokens—which contain more information—toward target visual regions, we compared the attention weights assigned to these regions by SAYO and Qwen3-VL when generating sequences with tokens of varying entropy levels. As shown in Figure 4, compared to the baseline model, SAYO maintains consistently high visual attention on most tokens with higher entropy, with lower

Table 3. Comparative results of visual attention reward for all generated tokens and key generated tokens on reasoning performance improvement.

Model	General				Math				Chart		Avg
	MMERealWorld	M3CoT	Vstar	MMStar	MathVision	We-Math	ChartQA	AI2D	CharXiv		
Qwen3-VL-8B	56.23	64.71	81.15	62.60	22.20	52.64	78.96	75.55	42.70	59.64	
	62.85	67.86	82.20	65.27	25.26	64.83	81.84	83.06	42.50	63.96	
	56.59	66.01	75.92	64.07	22.57	58.39	82.00	77.43	41.60	60.51	
InternVL3.5-8B	45.34	54.70	73.82	60.27	13.82	20.06	79.12	73.22	34.10	50.49	
	50.03	57.20	72.77	62.73	13.62	25.23	82.28	76.88	43.20	53.77	
	46.64	55.22	72.77	63.40	13.75	24.20	81.80	74.79	41.90	52.72	

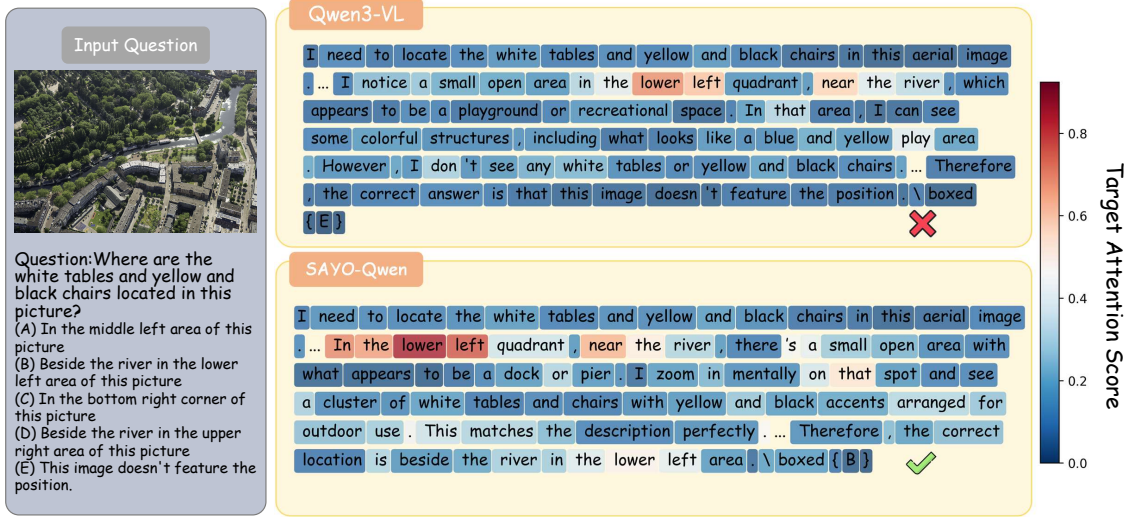


Figure 5. An example demonstrating how areas of visual attention shift during the reasoning process. The background color of tokens in the figure indicates the magnitude of the target visual attention score.

visual attention only observed on tokens with extremely low entropy and minimal information content.

As discussed in previous sections, the model itself possesses sufficient reasoning capabilities, with performance limitations primarily stemming from deficiencies in focusing attention on relevant visual information. Our proposed method enhances reasoning performance by strengthening the model's attention to effective visual information. Figure 5 presents a comprehensive example demonstrating that these gains are indeed due to the model's visual focus ability. In this example, SAYO correctly identified and focused on the object mentioned in the problem during the early stages of reasoning, and consistently maintained high visual attention weighting on that region at critical junctures of the reasoning process. This demonstrates the true key mechanism for visual problem reasoning. As shown in Figure 5, sustained and accurate visual attention can continuously guide the reasoning process away from erroneous visual information, thereby arriving at the correct conclusion. In summary, SAYO demonstrates a more precise focus on vi-

sual information. Experimental results also indicate that this feature enhances the accuracy of visual reasoning.

6. Conclusion

In this paper, we propose that the key factor influencing the reasoning performance of visual models is their ability to perceive and focus on critical visual information. Through quantitative research, we reveal that existing models exhibit poor attention to visual regions containing critical information for inference. We analyze the relationship between visual attention and inference accuracy: visual attention significantly impacts a model's reasoning accuracy. To address this key bottleneck, we propose a region-level visual attention enhancement training strategy: integrating token-level visual attention rewards into reinforcement learning training. This training strategy enhances model reasoning performance across multiple benchmarks, validating that precise visual attention effectively improves model capabilities.

Impact Statement

This paper presents work whose goal is to advance the field of Machine Learning. There are many potential societal consequences of our work, none which we feel must be specifically highlighted here.

References

Bai, S., Cai, Y., Chen, R., Chen, K., Chen, X., Cheng, Z., Deng, L., Ding, W., Gao, C., Ge, C., Ge, W., Guo, Z., Huang, Q., Huang, J., Huang, F., Hui, B., Jiang, S., Li, Z., Li, M., Li, M., Li, K., Lin, Z., Lin, J., Liu, X., Liu, J., Liu, C., Liu, Y., Liu, D., Liu, S., Lu, D., Luo, R., Lv, C., Men, R., Meng, L., Ren, X., Ren, X., Song, S., Sun, Y., Tang, J., Tu, J., Wan, J., Wang, P., Wang, P., Wang, Q., Wang, Y., Xie, T., Xu, Y., Xu, H., Xu, J., Yang, Z., Yang, M., Yang, J., Yang, A., Yu, B., Zhang, F., Zhang, H., Zhang, X., Zheng, B., Zhong, H., Zhou, J., Zhou, F., Zhou, J., Zhu, Y., and Zhu, K. Qwen3-vl technical report, 2025. URL <https://arxiv.org/abs/2511.21631>.

Cai, M., Liu, H., Mustikovela, S. K., Meyer, G. P., Chai, Y., Park, D., and Lee, Y. J. Making large multimodal models understand arbitrary visual prompts. In *IEEE Conference on Computer Vision and Pattern Recognition*, 2024.

Chen, C., Liu, M., Jing, C., Zhou, Y., Rao, F., Chen, H., Zhang, B., and Shen, C. Perturbollava: Reducing multimodal hallucinations with perturbative visual training, 2025. URL <https://arxiv.org/abs/2503.06486>.

Chen, L., Li, J., Dong, X., Zhang, P., Zang, Y., Chen, Z., Duan, H., Wang, J., Qiao, Y., Lin, D., and Zhao, F. Are we on the right way for evaluating large vision-language models?, 2024a. URL <https://arxiv.org/abs/2403.20330>.

Chen, Q., Qin, L., Zhang, J., Chen, Z., Xu, X., and Che, W. M³cot: A novel benchmark for multi-domain multi-step multi-modal chain-of-thought, 2024b. URL <https://arxiv.org/abs/2405.16473>.

Comanici, G., Bieber, E., Schaeckermann, M., and et al. Gemini 2.5: Pushing the frontier with advanced reasoning, multimodality, long context, and next generation agentic capabilities, 2025. URL <https://arxiv.org/abs/2507.06261>.

Deng, Y., Bansal, H., Yin, F., Peng, N., Wang, W., and Chang, K.-W. Openvlthinker: An early exploration to complex vision-language reasoning via iterative self-improvement, 2025. URL <https://arxiv.org/abs/2503.17352>.

Fu, X., Hu, Y., Li, B., Feng, Y., Wang, H., Lin, X., Roth, D., Smith, N. A., Ma, W.-C., and Krishna, R. Blink: Multimodal large language models can see but not perceive, 2024. URL <https://arxiv.org/abs/2404.12390>.

Fu, X., Liu, M., Yang, Z., Corring, J., Lu, Y., Yang, J., Roth, D., Florencio, D., and Zhang, C. Refocus: Visual editing as a chain of thought for structured image understanding, 2025. URL <https://arxiv.org/abs/2501.05452>.

Hu, Y., Shi, W., Fu, X., Roth, D., Ostendorf, M., Zettlemoyer, L., Smith, N. A., and Krishna, R. Visual sketchpad: Sketching as a visual chain of thought for multimodal language models. In Globerson, A., Mackey, L., Belgrave, D., Fan, A., Paquet, U., Tomczak, J., and Zhang, C. (eds.), *Advances in Neural Information Processing Systems*, volume 37, pp. 139348–139379. Curran Associates, Inc., 2024. doi: 10.52202/079017-4423.

Huang, A., Yao, C., Han, C., Wan, F., Guo, H., Lv, H., Zhou, H., Wang, J., Zhou, J., Sun, J., Hu, J., Lin, K., Zhao, L., Huang, M., Yuan, S., Qu, W., Wang, X., Lai, Y., Zhao, Y., Zhang, Y., Shi, Y., Chen, Y., Weng, Z., Meng, Z., Li, A., Kong, A., Dong, B., Wan, C., Wang, D., Qi, D., Li, D., Yu, E., Li, G., Yin, H., Zhou, H., Zhang, H., Yan, H., Zhou, H., Peng, H., Zhang, J., Lv, J., Fu, J., Cheng, J., Zhou, J., Yin, J., Xie, J., Wu, J., Zhang, J., Liu, J., Tan, K., Yan, K., Chen, L., Chen, L., Li, M., Zhao, Q., Sun, Q., Pang, S., Fan, S., Shang, S., Zhang, S., You, T., Ji, W., Xie, W., Yang, X., Hou, X., Jiao, X., Ren, X., Kong, X., Huang, X., Wu, X., Chen, X., Wang, X., Zhang, X., Wei, Y., Li, Y., Xu, Y., Shen, Y., Peng, Y., Peng, Y., Zhou, Y., Li, Y., Yang, Y., Zhang, Y., Xie, Z., Huang, Z., Lu, Z., Fan, Z., Cheng, Z., Jiang, D., Han, Q., Zhang, X., Zhu, Y., and Ge, Z. Step3-vl-10b technical report, 2026. URL <https://arxiv.org/abs/2601.09668>.

Hudson, D. A. and Manning, C. D. Gqa: A new dataset for real-world visual reasoning and compositional question answering. In *Proceedings of the IEEE/CVF Conference on Computer Vision and Pattern Recognition (CVPR)*, June 2019.

Jian, P., Wu, J., Sun, W., Wang, C., Ren, S., and Zhang, J. Look again, think slowly: Enhancing visual reflection in vision-language models, 2025. URL <https://arxiv.org/abs/2509.12132>.

Kembhavi, A., Salvato, M., Kolve, E., Seo, M., Hajishirzi, H., and Farhadi, A. A diagram is worth a dozen images. In *Computer Vision – ECCV 2016*, pp. 235–251, Cham, 2016. Springer International Publishing.

Liu, X., Ni, J., Wu, Z., Du, C., Dou, L., Wang, H., Pang, T., and Shieh, M. Q. Noisyrollout: Reinforcing visual

reasoning with data augmentation, 2025a. URL <https://arxiv.org/abs/2504.13055>.

Liu, Z., Chen, Z., Liu, H., Luo, C., Tang, X., Wang, S., Zeng, J., Dai, Z., Shi, Z., Wei, T., Dumoulin, B., and Tong, H. Seeing but not believing: Probing the disconnect between visual attention and answer correctness in vlms, 2025b. URL <https://arxiv.org/abs/2510.17771>.

Masry, A., Long, D. X., Tan, J. Q., Joty, S., and Hoque, E. ChartQA: A benchmark for question answering about charts with visual and logical reasoning. In *Findings of the Association for Computational Linguistics: ACL 2022*, pp. 2263–2279, Dublin, Ireland, May 2022. Association for Computational Linguistics. doi: 10.18653/v1/2022.findings-acl.177.

OpenAI. Hello gpt-4o. URL <https://openai.com/index/Hello-gpt-4o/>.

Qiao, R., Tan, Q., Dong, G., MinhuiWu, M., Sun, C., Song, X., Wang, J., GongQue, Z., Lei, S., Zhang, Y., Wei, Z., Zhang, M., Qiao, R., Zong, X., Xu, Y., Yang, P., Bao, Z., Diao, M., Li, C., and Zhang, H. We-math: Does your large multimodal model achieve human-like mathematical reasoning? In *Proceedings of the 63rd Annual Meeting of the Association for Computational Linguistics (Volume 1: Long Papers)*. Association for Computational Linguistics, July 2025. doi: 10.18653/v1/2025.acl-long.983.

Sarch, G., Saha, S., Khandelwal, N., Jain, A., Tarr, M. J., Kumar, A., and Fragkiadaki, K. Grounded reinforcement learning for visual reasoning, 2025. URL <https://arxiv.org/abs/2505.23678>.

Shao, Z., Wang, P., Zhu, Q., Xu, R., Song, J., Bi, X., Zhang, H., Zhang, M., Li, Y. K., Wu, Y., and Guo, D. Deepseekmath: Pushing the limits of mathematical reasoning in open language models, 2024. URL <https://arxiv.org/abs/2402.03300>.

Team, K., Du, A., Yin, B., Xing, B., Qu, B., Wang, B., Chen, C., Zhang, C., Du, C., Wei, C., Wang, C., Zhang, D., Du, D., Wang, D., Yuan, E., Lu, E., Li, F., Sung, F., Wei, G., Lai, G., Zhu, H., Ding, H., Hu, H., Yang, H., Zhang, H., Wu, H., Yao, H., Lu, H., Wang, H., Gao, H., Zheng, H., Li, J., Su, J., Wang, J., Deng, J., Qiu, J., Xie, J., Wang, J., Liu, J., Yan, J., Ouyang, K., Chen, L., Sui, L., Yu, L., Dong, M., Dong, M., Xu, N., Cheng, P., Gu, Q., Zhou, R., Liu, S., Cao, S., Yu, T., Song, T., Bai, T., Song, W., He, W., Huang, W., Xu, W., Yuan, X., Yao, X., Wu, X., Zu, X., Zhou, X., Wang, X., Charles, Y., Zhong, Y., Li, Y., Hu, Y., Chen, Y., Wang, Y., Liu, Y., Miao, Y., Qin, Y., Chen, Y., Bao, Y., Wang, Y., Kang, Y., Liu, Y., Du, Y., Wu, Y., Wang, Y., Yan, Y., Zhou, Z., Li, Z., Jiang, Z., Zhang, Z., Yang, Z., Huang, Z., Huang, Z., Zhao, Z., and Chen, Z. Kimi-VL technical report, 2025. URL <https://arxiv.org/abs/2504.07491>.

Tong, S., Liu, Z., Zhai, Y., Ma, Y., LeCun, Y., and Xie, S. Eyes wide shut? exploring the visual shortcomings of multimodal llms, 2024. URL <https://arxiv.org/abs/2401.06209>.

Verma, G., Choi, M., Sharma, K., Watson-Daniels, J., Oh, S., and Kumar, S. Cross-modal projection in multimodal llms doesn't really project visual attributes to textual space, 2024. URL <https://arxiv.org/abs/2402.16832>.

von Werra, L., Belkada, Y., Tunstall, L., Beeching, E., Thrush, T., Lambert, N., Huang, S., Rasul, K., and Gallouédec, Q. Trl: Transformer reinforcement learning. <https://github.com/huggingface/trl>, 2020.

Wang, J., Liu, Z., Rao, Y., and Lu, J. Sparsemm: Head sparsity emerges from visual concept responses in mllms, 2025a. URL <https://arxiv.org/abs/2506.05344>.

Wang, K., Pan, J., Shi, W., Lu, Z., Ren, H., Zhou, A., Zhan, M., and Li, H. Measuring multimodal mathematical reasoning with math-vision dataset. In Globerson, A., Mackey, L., Belgrave, D., Fan, A., Paquet, U., Tomczak, J., and Zhang, C. (eds.), *Advances in Neural Information Processing Systems*, volume 37, pp. 95095–95169. Curran Associates, Inc., 2024a. doi: 10.52202/079017-3014.

Wang, S., Yu, L., Gao, C., Zheng, C., Liu, S., Lu, R., Dang, K., Chen, X., Yang, J., Zhang, Z., Liu, Y., Yang, A., Zhao, A., Yue, Y., Song, S., Yu, B., Huang, G., and Lin, J. Beyond the 80/20 rule: High-entropy minority tokens drive effective reinforcement learning for llm reasoning, 2025b. URL <https://arxiv.org/abs/2506.01939>.

Wang, W., Gao, Z., Gu, L., Pu, H., Cui, L., Wei, X., Liu, Z., Jing, L., Ye, S., Shao, J., Wang, Z., Chen, Z., Zhang, H., Yang, G., Wang, H., Wei, Q., Yin, J., Li, W., Cui, E., Chen, G., Ding, Z., Tian, C., Wu, Z., Xie, J., Li, Z., Yang, B., Duan, Y., Wang, X., Hou, Z., Hao, H., Zhang, T., Li, S., Zhao, X., Duan, H., Deng, N., Fu, B., He, Y., Wang, Y., He, C., Shi, B., He, J., Xiong, Y., Lv, H., Wu, L., Shao, W., Zhang, K., Deng, H., Qi, B., Ge, J., Guo, Q., Zhang, W., Zhang, S., Cao, M., Lin, J., Tang, K., Gao, J., Huang, H., Gu, Y., Lyu, C., Tang, H., Wang, R., Lv, H., Ouyang, W., Wang, L., Dou, M., Zhu, X., Lu, T., Lin, D., Dai, J., Su, W., Zhou, B., Chen, K., Qiao, Y., Wang, W., and Luo, G. Internvl3.5: Advancing open-source multimodal models in versatility, reasoning, and efficiency, 2025c. URL <https://arxiv.org/abs/2508.18265>.

Wang, Z., Xia, M., He, L., Chen, H., Liu, Y., Zhu, R., Liang, K., Wu, X., Liu, H., Malladi, S., Chevalier, A., Arora, S., and Chen, D. Charxiv: Charting gaps in realistic chart understanding in multimodal llms. In Globerson, A., Mackey, L., Belgrave, D., Fan, A., Paquet, U., Tomczak, J., and Zhang, C. (eds.), *Advances in Neural Information Processing Systems*, volume 37, pp. 113569–113697. Curran Associates, Inc., 2024b. doi: 10.52202/079017-3609.

Wu, M., Cai, X., Ji, J., Li, J., Huang, O., Luo, G., Fei, H., Jiang, G., Sun, X., and Ji, R. Controlmllm: Training-free visual prompt learning for multimodal large language models, 2025. URL <https://arxiv.org/abs/2407.21534>.

Wu, P. and Xie, S. V?: Guided visual search as a core mechanism in multimodal llms. In *Proceedings of the IEEE/CVF Conference on Computer Vision and Pattern Recognition (CVPR)*, pp. 13084–13094, June 2024.

Xu, G., Jin, P., Li, H., Song, Y., Sun, L., and Yuan, L. Llava-cot: Let vision language models reason step-by-step, 2025. URL <https://arxiv.org/abs/2411.10440>.

Yang, S., Gao, Z., Qiu, H., Liu, F., Shi, P., Zeng, Z., Liao, Q., and Ma, L. Learning when to look: A disentangled curriculum for strategic perception in multimodal reasoning, 2025a. URL <https://arxiv.org/abs/2512.17227>.

Yang, S., Niu, Y., Liu, Y., Ye, Y., Lin, B., and Yuan, L. Look-back: Implicit visual re-focusing in mllm reasoning, 2025b. URL <https://arxiv.org/abs/2507.03019>.

Yang, Y., He, X., Pan, H., Jiang, X., Deng, Y., Yang, X., Lu, H., Yin, D., Rao, F., Zhu, M., Zhang, B., and Chen, W. R1-onevision: Advancing generalized multimodal reasoning through cross-modal formalization. *arXiv preprint arXiv:2503.10615*, 2025c.

Yang, Z., Li, L., Wang, J., Lin, K., Azarnasab, E., Ahmed, F., Liu, Z., Liu, C., Zeng, M., and Wang, L. Mm-react: Prompting chatgpt for multimodal reasoning and action, 2023. URL <https://arxiv.org/abs/2303.11381>.

Zhang, J., Khayatkhoei, M., Chhikara, P., and Ilievski, F. Mllms know where to look: Training-free perception of small visual details with multimodal llms, 2025a. URL <https://arxiv.org/abs/2502.17422>.

Zhang, Y.-F., Zhang, H., Tian, H., Fu, C., Zhang, S., Wu, J., Li, F., Wang, K., Wen, Q., Zhang, Z., Wang, L., Jin, R., and Tan, T. Mme-realworld: Could your multimodal llm challenge high-resolution real-world scenarios that are difficult for humans?, 2025b. URL <https://arxiv.org/abs/2408.13257>.

A. Implementation of Training Details and Hyperparameters

During the Group Relative Policy Optimization (GRPO) phase, we limit max responses to 110 tokens and apply KL divergence with a coefficient of $1e^{-3}$. We use 6 GPUs with 4 epochs of training. More details and hyperparameters are shown in Table 4

Table 4. The hyperparameters used during GRPO with visual attention based reward.

Parameters	Value
Epochs	4
Per Device Batch Size	64
Warmup	False
Rollout	16
Rollout Temperature	1.0
Rollout Top-P	0.9
KL divergence coefficient	1×10^{-3}
Learning rate	5×10^{-6}
Weight Decay	1×10^{-2}
Max Grad Norm	0.8
Optimizer	AdamW

B. Prompts in Training and Evaluation

Prompt Template in GRPO

A conversation between a user and an assistant. The user asks a question, and the assistant must answer it. The assistant first conducts internal reasoning, followed immediately by the final answer enclosed within `<answer>...</answer>` tags.

Requirements:

1. The reasoning outside `<answer></answer>` should be concise, minimal, and essential.
2. The final answer must be correct, complete, and directly address the user's question.
3. When reasoning, focus on the areas of aim object in the image.

`<question>`

Prompt Template in Evaluation

You FIRST think about the reasoning process as an internal monologue and then provide the final answer. The reasoning process MUST BE enclosed within `<think> </think>` tags. The final answer MUST BE put in boxed{ }.

C. Training Data Source

We collected data from the dataset in the field of real-world visual reasoning and the structured graph reasoning for RL training. The specific composition is shown in Table 5.

Datasets	Size
GQA (Hudson & Manning, 2019)	$\sim 16k$
Refocus_Data (Fu et al., 2025)	$\sim 4k$

Table 5. Detailed composition of the datasets used for RL

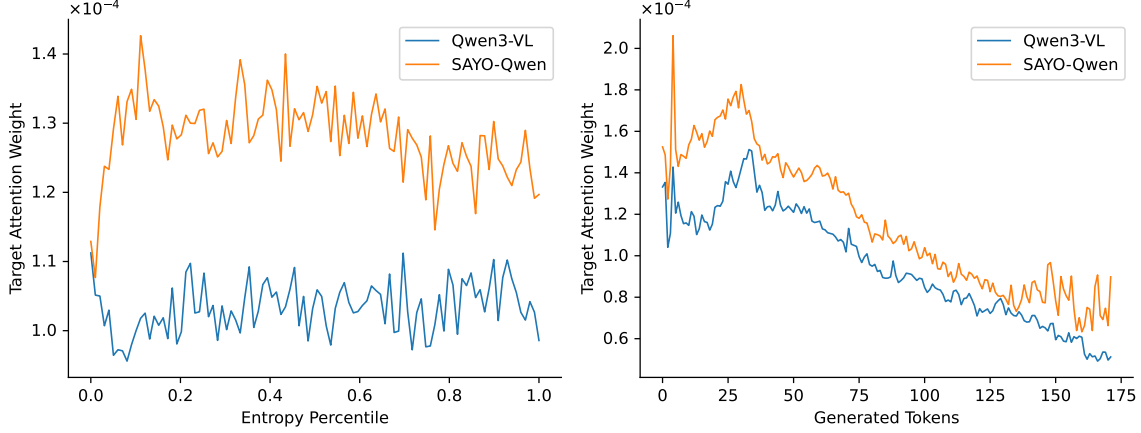


Figure 6. Attention weight (last layer) on target visual token in Qwen3-VL-8B-Instruct and SAYO-8B. The entropy values shown have been normalized across samples, and the displayed attention weights represent the average across all samples.

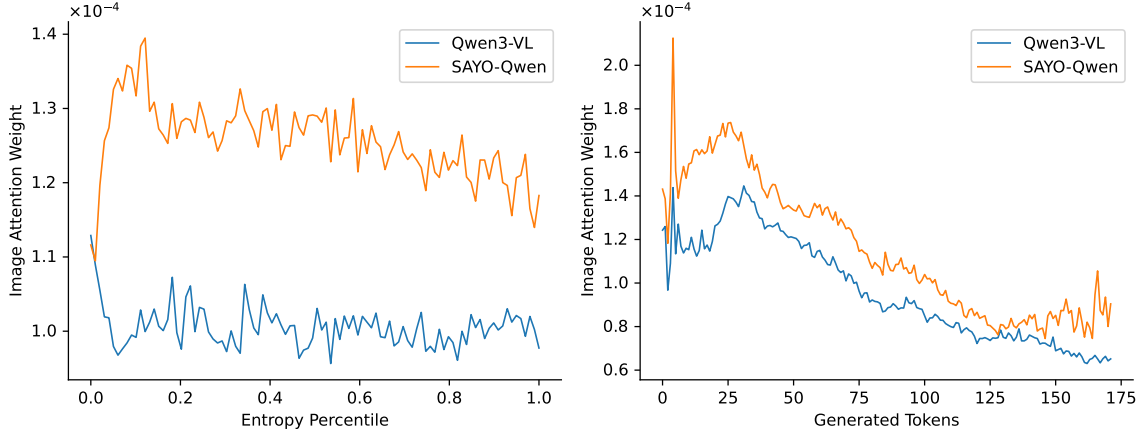


Figure 7. Attention weight (last layer) on all visual tokens in Qwen3-VL-8B-Instruct and SAYO-8B. The entropy values shown have been normalized across samples, and the displayed attention weights represent the average across all samples.

D. Experiments Results

Detailed Study of Visual Attention Shifts We further evaluated SAYO’s optimization of visual attention on the test dataset. As shown in Figures 6 and 7, SAYO maintains higher attention to both the target region and the entire image throughout the generation process compared to baseline models. When comparing tokens with different entropies, SAYO significantly enhances visual attention for all tokens except those with extremely low entropy.

Detailed Study of Entropy Sensitivity To further investigate the impact of entropy selection range on attention rewards, we trained multiple entropy-based reward token selection ranges. As shown in Table 6, selecting fewer tokens will exclude some tokens carrying important information, leading to reduced training effectiveness. Conversely, selecting more tokens introduces additional training noise, thereby diminishing training outcomes.

Improvement in Model Inference Length Figure 8 illustrates the relationship between model output length and accuracy across different benchmarks. Thanks to improved visual attention, SAYO achieves higher reasoning performance with shorter reasoning lengths.

Table 6. Ablation results for different ranges of entropy select strategies in visual attention-based reward.

Range	General		Math		Chart	
	MMERealWorld	M3CoT	MathVision	We-Math	AI2D	CharXiv
Sayo-Qwen-8B	62.85	68.46	25.26	64.83	83.06	42.50
Top 20% tokens	58.36	65.19	17.80	59.08	79.40	40.90
Top 40% tokens	62.48	66.18	20.13	66.84	82.93	39.30

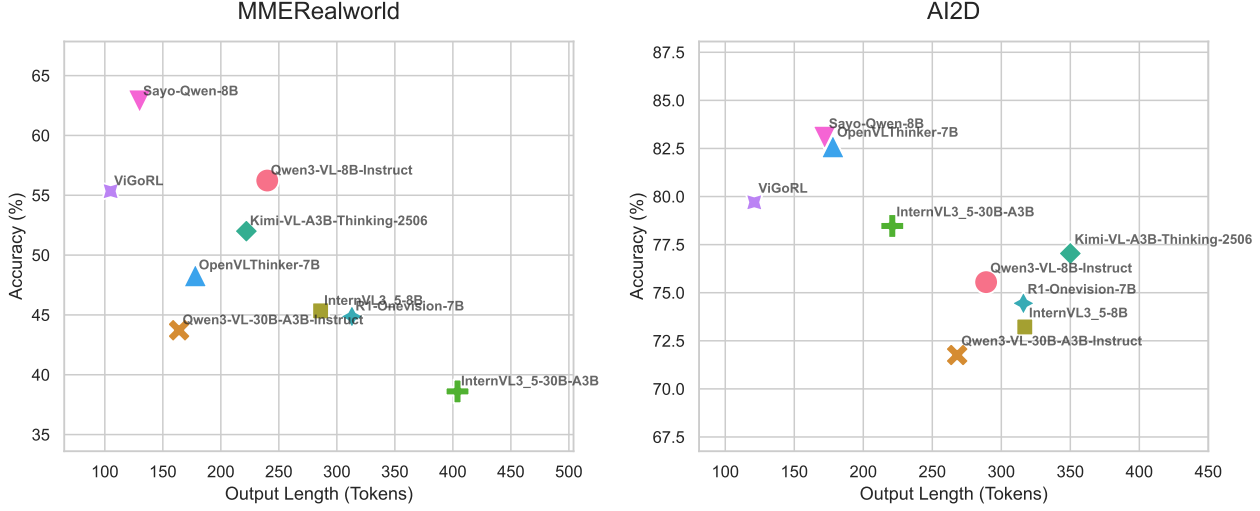


Figure 8. Comparative analysis of model accuracy and average output length across MMERealworld and AI2D.

E. Training Behaviors

Figure 9 shows the training details for selecting top token rewards versus full token rewards. After excluding low-entropy tokens, the reward values can increase normally during training due to reduced noise signals.

F. Case Study

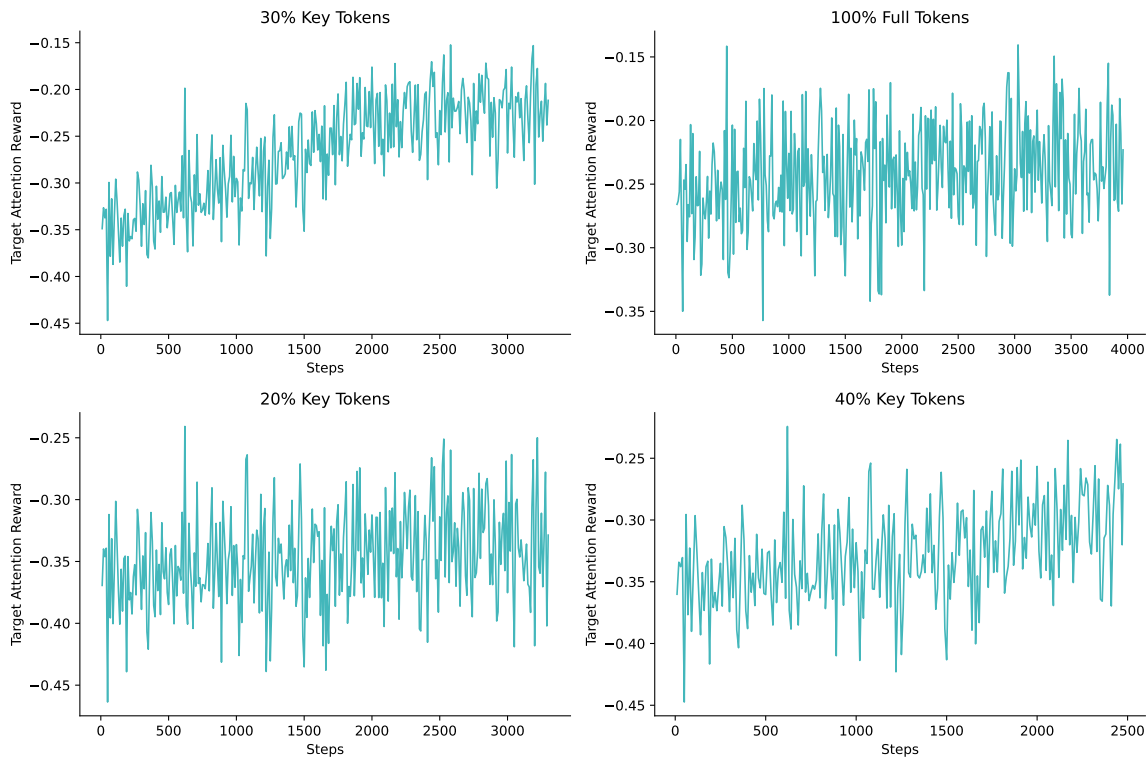


Figure 9. Attention rewards vary with training step. The left figure shows rewards covering the top 30% of high-entropy tokens, while the right figure covers all tokens.

Question: Is the value of light green bar 35 in 1989?

Qwen3VL

Can the European Parliament's center hold?

Share of members of the European Parliament belonging to parties or political groups

	Green or regionalist				
	Left-wing to far left	Center-left	Centrist	Center-right	Right-wing to far right
1979	12%	27%	11%	42%	7% 1%
1984	10	30	7	37	11 5
1989	8	35	10	30	9 8
1994	5	35	11	30	14 5
1999	7	29	9	37	9 8
2004	6	28	13	37	11 6
2009	5	25	12	36	15 7
2014	7	25	9	29	20 7

Note: Figures are as of each parliament's initial organizing session following EU-wide elections. Off-year results not shown. Two national parties represented in the current European Parliament (Italy's Five Star Movement and a German satirical party) have platforms that are too heterogeneous to categorize; they were not included in the 2014 figures above.

Source: Pew Research Center analysis of European Parliament election data.

PEW RESEARCH CENTER

To determine if the value of the light green bar is 35 in 1989, I need to examine the provided bar chart.

- **Locate the year 1989:** I find the row labeled "1989" in the chart.
- **Identify the light green bar:** The legend at the top indicates that the "Left-wing to far left" category is represented by the light green bar.
- **Read the value for 1989:** Looking at the "1989" row, the light green bar (Left-wing to far left) has the value "8" written inside it.

The value shown for the light green bar in 1989 is 8, not 35. The value 35 is in the same row but corresponds to the "Center-left" category, which is represented by a darker green bar.

Therefore, the statement is false.

\boxed{No}

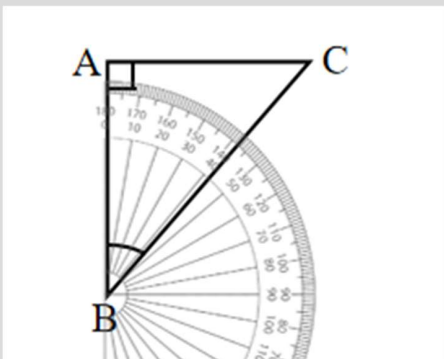
Sayo-Qwen

I need to examine the chart to find the light green bar corresponding to the year 1989. The light green bar represents the "Center-left" political group. Looking at the row for 1989, I see that the light green bar has a value of 35, which is clearly labeled in the chart. This value is consistent with the trend shown in the chart for the center-left group, which was relatively strong in the 1980s and early 1990s before declining slightly in later years. The value is also visually distinct from the other bars in that row.

\boxed{Yes}

Figure 10. Case 1 of Sayo-Qwen-8B in ChartQA.

Question: As shown in the figure, the protractor measures the degree of $\angle B$ as ()°?
Options: A. 42; B. 50; C. 60; D. No correct answer



Qwen3VL

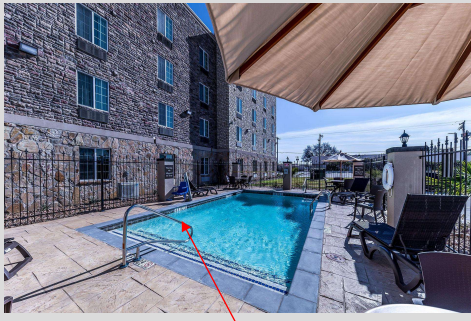
Looking at the figure, I see a right triangle ABC with the right angle at A. There is a protractor centered at point B, and it's measuring angle ABC, which is angle B. The protractor has two scales: the outer one going from 0° to 180° clockwise, and the inner one going from 0° to 180° counterclockwise. Since the angle is at the vertex B, and the rays go out to A and C, I need to see which scale to read. Looking at the protractor, the ray BA is aligned with the 0° mark on the outer scale (which is the one going from 0° to 180° clockwise). The ray BC is pointing to the 50° mark on the outer scale. Therefore, the measure of angle ABC is 50°. Let me double-check. The protractor is centered at B. The baseline (0°) is along BA. The ray BC is at 50° on the outer scale. Since the angle is inside the triangle and the protractor is oriented such that the 0° is on BA and the 180° is on the opposite side, the angle between BA and BC is indeed 50°. So, the answer should be 50°. \boxed{B}

Sayo-Qwen

I need to determine the measure of angle B using the protractor shown in the figure. The protractor is centered at point B, and the angle is formed by rays BA and BC. The protractor has two scales: the outer one going from 0° to 180° clockwise, and the inner one going counterclockwise. Since point A is at the 0° mark on the outer scale, and point C is somewhere along the arc, I need to read the angle from the outer scale. Looking at the protractor, the ray BC intersects the outer scale at approximately 42 degrees. The inner scale would read 138 degrees, but since the angle is measured from the 0° mark at A, we use the outer scale. The arc from A to C clearly aligns with the 42° mark on the outer scale. The right angle at A confirms that this is a right triangle, but the question is specifically about angle B. Therefore, the measure of angle B is 42 degrees. \boxed{A}

Figure 11. Case 2 of Sayo-Qwen-8B in We-Math

Question: What's the text on the pool by the blue chair?
Choices: (A) 4FT12, (B) 7FT12, (C) 4FT13, (D) 4FT11, (E) The image doesn't feature the content.



Qwen3VL

I need to examine the image closely to find the text on the pool near the blue chair. The blue chair is on the left side of the pool, next to a metal handrail. There is a small white sign with black text on the pool deck right next to the handrail, near the blue chair. Looking at the sign, I can clearly read the text: "4FT11". This appears to be a depth marker indicating the water depth at that point is 4 feet 11 inches. Now, I will compare this to the given choices:- (A) 4FT12- (B) 7FT12- (C) 4FT13- (D) 4FT11- (E) The image doesn't feature the content. The text on the sign matches option (D) 4FT11.
\boxed{D}

Sayo-Qwen

I need to examine the text on the pool near the blue chair. The blue chair is on the left side of the pool, next to the metal handrail. Looking closely at the pool's edge near that area, there's a small white sign with black lettering. The sign is partially visible and appears to read "4FT12" — indicating a depth of 4 feet 12 inches. This matches the depth marker commonly placed on pool edges for safety. The other options don't align with the visible text. The image clearly shows the text, so the correct choice is not "the image doesn't feature the content."
\boxed{(A) 4FT12}

Figure 12. Case 3 of Sayo-Qwen-8B in MME-Realworld